Zero-Crossing Modulations for a Multi-User MIMO Downlink with 1-Bit Temporal Oversampling ADCs

Peter Neuhaus*, Diana M. V. Melo†, Lukas T. N. Landau†, Rodrigo C. de Lamare†, and Gerhard Fettweis*
*Vodafone Chair Mobile Communications Systems, Technische Universität Dresden, 01062 Dresden, Germany
†Centre for Telecommunications Studies, Pontifical Catholic University of Rio de Janeiro, Rio de Janeiro, Brazil 22453-900
Email: {peter_friedrich.neuhaus, gerhard.fettweis}@tu-dresden.de, {diana, lukas.landau, delamare}@cetuc.puc-rio.br

***Abstract*—The use of low-resolution quantization is a promising approach to reduce the power consumption of the analog-to-digital converters (ADCs) of future wireless communications systems. In this work, we investigate a multi-user MIMO downlink scenario with 1-bit quantization and temporal oversampling at the receivers. The information is encoded in the zero-crossings (ZXs) in such systems, a concept which is known as zero-crossing modulation (ZXM). ZXM could enable energy-efficient communications in the internet of things (IoT) or wideband systems operating on millimeter-wave and terahertz bands. Here, we compare two practical ZXM waveform mappings in terms of their uncoded bit error rate and evaluate a lower bound on their spectral efficiency when employing minimum mean squared error (MMSE) precoding.**

***Index Terms*—1-bit, quantization, oversampling, precoding**

I. Introduction

Beyond 5G systems are foreseen to support a massive number of internet of things (IoT) devices, operating at low data rates [1]. Such scenarios require low-cost devices with battery lifetimes in the order of several years. Employing 1-bit quantization at the receiver could enable simple low-cost energy-efficient receivers for such systems because the analog-to-digital converter (ADC) power consumption typically grows exponentially in the number of bits [2], i. e., in the amplitude resolution.

Some of the loss due to 1-bit quantization can be compensated for by employing temporal oversampling w. r. t. the Nyquist rate. In [3] it has been shown that rates of $\log_2(M_{\mathrm{Rx}} + 1)$ bits per Nyquist interval are achievable in the noiseless case by M_{Rx}-fold oversampling. The authors of [4] propose and evaluate a practical system concept based on the idea from [3] and show that similar rates can also be achieved over noisy channels. Lower bounds on the achievable rate for a large number of transmit signal designs tailored to systems employing 1-bit quantization and temporal oversampling have been evaluated in [5]. Employing runlength-limited (RLL) sequence transmit signals, as first proposed in [6], has been found promising therein. A practical implementation of a system employing 1-bit quantization and temporal oversampling in combination with RLL transmit sequences has been evaluated in [7], [8].

The gain of employing oversampling in a 1-bit quantized massive multiple-input multiple-output (MIMO) uplink scenario has been investigated in [9]. In [10] it has been shown that in wideband systems temporal oversampling can achieve a similar performance as spatial oversampling at a reduced complexity. Spatio-temporal precoding for a multi-user massive MIMO downlink, where the receivers employ 1-bit quantization and temporal oversampling, has been studied in [11]. Two superior bit mappings and precoding schemes for the same scenario have been investigated in [12], [13].

In this work, we consider the same multi-user MIMO downlink scenario as in [11]–[13], where the receivers employ 1-bit quantization and temporal oversampling. Furthermore, we utilize the spatio-temporal minimum mean squared error (MMSE) precoder from [13]. For this setup, we compare two practical mappings from bits onto zero-crossings (ZXs) to implement zero-crossing modulation (ZXM) [14]. The considered mappings are: *i*) The time-instance ZX mapping from [13], and *ii*) the RLL sequence based mapping which has been derived in [7]. Furthermore, instead of using the soft-input soft-output RLL decoder from [7], we present a low-complexity minimum Hamming distance *Viterbi algorithm* for RLL sequence decoding. Moreover, in contrast to the prior works [12], [13], we propose and numerically evaluate a simple spectral efficiency (SE) lower bound, which depends on the system's uncoded bit error rate (BER). Finally, we show numerically that the considered ZX mappings significantly outperform the quantization precoding (QP) from [11] at low signal-to-noise ratios (SNRs).

The remainder of this paper is organized as follows: First, we briefly review the two considered ZX mappings in Sec. II. Then we detail the system model, spatio-temporal MMSE precoding, and minimum Hamming distance detection in Sec. III. Afterwards, in Sec. IV, we derive a simple lower bound on the system's SE. Numerical results are presented in Sec. V. Finally, our work is concluded in Sec. VI.

Notation: Vectors and matrices are denoted by lower and uppercase boldface letters, i. e., $\boldsymbol{x}$ and $\boldsymbol{X}$, respectively. The nth element of the vector $\boldsymbol{x}$, i. e., a scalar quantity, is denoted as $x_n = [\boldsymbol{x}]_n$. The identity matrix of size $N \times N$ is written as $\boldsymbol{I}_N$. Moreover, expectation, trace and Kronecker product operations are denoted by $\mathbb{E}\{\cdot\}$, $\mathrm{tr}\{\cdot\}$ and $\otimes$, respectively.

II. Zero-Crossing Mappings

In this section, we briefly review two existing practical ZX mappings for systems employing 1-bit quantization and temporal oversampling at the receiver. Both ZX mappings are subsequently used in Sec. III to independently modulate the in-phase and quadrature component of the transmit signal.

This work has been supported in part by the German Federal Ministry of Education and Research (BMBF) (project E4C, contract number 16ME0189), in part by the ELIOT ANR18-CE40-0030 project, and in part by the FAPESP 2018/12579-7 project.

A. Time-Instance Zero-Crossing Mapping

A time-instance ZX mapping has been proposed in [12], [13]. It is designed for receivers employing 1-bit quantization and M_{Rx}-fold oversampling, such that each Nyquist interval is associated with M_{Rx} binary samples. The receiver can detect ZXs in one of the M_{Rx} sub-intervals or the absence of a ZX, hence, resulting in $M_{\mathrm{Rx}}+1$ unique patterns per Nyquist interval. This implies that the information is conveyed in the ZX time-instances per Nyquist interval.

For $M_{\mathrm{Rx}}=3$, to encode the ith Nyquist interval, the encoder maps two input bits onto one of the $M_{\mathrm{Rx}}+1=4$ possible ZX patterns $\boldsymbol{c}_{\mathrm{s},i}$ (cf. [13, Table II]). Each Nyquist interval is associated with two possible codewords $\boldsymbol{c}_{\mathrm{s},i}$, since the ZX may be from positive to negative amplitudes or vice versa. Consequently, the pattern of each segment $\boldsymbol{c}_{\mathrm{s},i}$ depends on the last sample p_{i-1} of the previous codeword $\boldsymbol{c}_{\mathrm{s},i-1}$. The employed time-instance ZX mapping codewords are listed in [13, Table I-II], where inputs and outputs are read from left-to-right. Note that in case of $M_{\mathrm{Rx}}=2$ (cf. [13, Table I]), three input bits are mapped onto ZXs over two consecutive Nyquist intervals, i. e., each $\boldsymbol{c}_{\mathrm{s},i}$ spans two Nyquist intervals.

Finally, for each user k, the combined transmit sequence $\boldsymbol{c}_{\mathrm{out}_k}=[p_{\mathrm{b}},\boldsymbol{c}_{\mathrm{s},0}^T,\ldots,\boldsymbol{c}_{\mathrm{s},N-1}^T]^T$ with total length $N_{\mathrm{tot}}=NM_{\mathrm{Rx}}+1$ is obtained by concatenating the segments $\boldsymbol{c}_{\mathrm{s},i}$. Given the dependency of the construction of $\boldsymbol{c}_{\mathrm{s},i}$ on the previous code segment $\boldsymbol{c}_{\mathrm{s},i-1}$, a single pilot symbol $p_{\mathrm{b}}\in\{1,-1\}$ is inserted at the beginning of the sequence to initialize the encoding and decoding.

B. Runlength-Limited Zero-Crossing Precoding

Using RLL sequences [15] for systems employing 1-bit quantization and temporal oversampling has been proposed in [5], [6]. They are a natural choice for such systems because the information is conveyed in the *temporal distance* between ZXs, which can be recovered after 1-bit quantization.

RLL sequences are discrete bipolar sequences, typically with amplitude ±1, which are constraint such that the minimum and maximum distance between two amplitude transitions is given by $d+1$ and $k+1$, respectively [15]. An example for an RLL sequence with constraint $(d=1,k=\infty)$ is given below:

$$\boldsymbol{c}_{\mathrm{out}_k}=[\ldots,+1,+1,+1,-1,-1,+1,+1,+1,-1,-1,\ldots]^T.$$

The minimum runlength constraint, also denoted as d-constraint, is introduced to reduce inter-symbol interference (ISI), whereas the maximum runlength constraint, also denoted as k-constraint, is introduced to ensure proper synchronization. The k-constraint is omitted here, i. e., we set $k=\infty$, as we do not consider synchronization. The reader is referred to [15] for more details on RLL sequences.

In this work, we employ the finite-state machine (FSM) RLL codes, which where derived in [7]. The encoder is initialized to a pre-defined state $s_0\in\mathcal{S}_{\mathrm{RLL}}$, where $\mathcal{S}_{\mathrm{RLL}}$ denotes the set of all encoder states. Then, depending on the current state s_0 and the current input block of p bits, the encoder produces an output RLL sequence block of length q and translates into a new state s_1. The procedure is repeated for each input block. The code rate is consequently given by $R_{\mathrm{RLL}}=p/q$. The encoders are specified in [7, Table I-II].

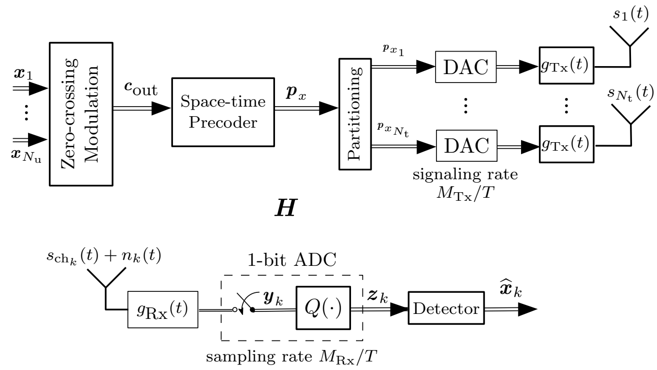

Fig. 1. Considered multi-user MIMO downlink system model.

C. Discussion

The encoding process for the time-instance ZX mapping depends on the last symbol of the previous codeword, hence, the encoder can also be considered as a FSM encoder with two internal states. Therefore, the encoders of both mappings are closely related. However, when comparing the encoding tables [13, Table I-II] and [7, Table I-II], we conclude that the encoding process for RLL sequences is more complex.

The different complexity is partly due to the significantly different distribution of the ZXs of the two considered mappings: The ZXs in the time-instance ZX mapping are approximately uniformly distributed (cf. [13, Table I-II]), whereas the considered FSM RLL codes approximate maximum entropy RLL sequences, where the ZXs follow a truncated geometric distribution [15]. Additionally, the RLL d-constraint reduces ISI, which is not the case for the time-instance ZX mapping.

III. System Model

In this work, we consider the multi-user MIMO downlink scenario from [11]–[13] consisting of a single base station (BS) with N_{t} antennas and N_{u} single-antenna users. The system model is depicted in Fig. 1. At the BS, the per-user bit vectors, denoted by $\boldsymbol{x}_k\in\{0,1\}^{I_{\mathrm{b}}}$, $I_{\mathrm{b}}\in\mathbb{N}$, $k\in\{1,\ldots,N_{\mathrm{u}}\}$, are first modulated using one of the considered ZX mappings (cf. Sec. II). The outputs of the ZX modulator are written as $\boldsymbol{c}_{\mathrm{out}_k}\in\mathbb{C}^{N_{\mathrm{tot}}}$. Afterwards, MMSE space-time precoding over blocks of N Nyquist intervals is employed, which yields the precoded per antenna streams $\boldsymbol{p}_{x_n}\in\mathbb{C}^{M_{\mathrm{Tx}}N+1}$, where M_{Tx}/T denotes the signaling rate and T denotes the Nyquist interval of the transmit filter. For $M_{\mathrm{Tx}}>1$ this implicitly corresponds to faster-than-Nyquist (FTN) signaling [16]. Transmit and receive filters are written as $g_{\mathrm{Tx}}(t)$ and $g_{\mathrm{Rx}}(t)$ respectively. Then, the combined transmit and receive filter is given by $v(t)=(g_{\mathrm{Tx}}*g_{\mathrm{Rx}})(t)$. Furthermore, we assume a frequency-flat fading channel, denoted by $\boldsymbol{H}\in\mathbb{C}^{N_{\mathrm{u}}\times N_{\mathrm{t}}}$, which is known at the BS.

The N_{u} receivers employ M_{Rx}-fold oversampling w. r. t. the Nyquist rate, such that the sampling rate is given by M_{Rx}/T.

Then, stacking the received samples of the N_u users *prior to quantization* yields the following vector of length $N_\text{u} N_\text{tot}$

$$\boldsymbol{y} = \boldsymbol{H}_\text{eff}\, \boldsymbol{p}_x + \boldsymbol{G}_\text{Rx,eff}\, \boldsymbol{n}, \tag{1}$$

where $\boldsymbol{p}_x \in \mathbb{C}^{N_\text{t}(M_\text{Tx} N+1)}$ represents the space-time precoding vector and $\boldsymbol{n} \in \mathbb{C}^{3N_\text{tot}N_\text{u}}$ denotes a zero-mean complex Gaussian noise vector with variance σ_n^2. Furthermore, $\boldsymbol{H}_\text{eff} = (\boldsymbol{H} \otimes \boldsymbol{I}_{N_\text{tot}})(\boldsymbol{I}_{N_\text{t}} \otimes \boldsymbol{V}\boldsymbol{U})$ and $\boldsymbol{G}_\text{Rx,eff} = (\boldsymbol{I}_{N_\text{u}} \otimes \boldsymbol{G}_\text{Rx})$ denote the effective channel and the effective receive filter matrices, respectively. They are defined using the waveform impulse response matrix $\boldsymbol{V}$ and the receive filter matrix $\boldsymbol{G}_\text{Rx}$, which are of size $N_\text{tot} \times N_\text{tot}$ and $N_\text{tot} \times 3N_\text{tot}$, respectively. The matrices are given by

$$\boldsymbol{V} = \begin{bmatrix} v\,(0) & v\left(\frac{T}{M_\text{Rx}}\right) & \cdots & v\,(TN) \\ v\left(-\frac{T}{M_\text{Rx}}\right) & v\,(0) & \cdots & v\left(T\left(N-\frac{1}{M_\text{Rx}}\right)\right) \\ \vdots & \vdots & \ddots & \vdots \\ v\,(-TN) & v\left(T\left(-N+\frac{1}{M_\text{Rx}}\right)\right) & \cdots & v\,(0) \end{bmatrix} \tag{2}$$

and

$$\boldsymbol{G}_\text{Rx} = a_\text{Rx} \begin{bmatrix} \left[\ \boldsymbol{g}_\text{Rx}^T\ \right] & 0 \cdots & 0 \\ 0 & \left[\ \boldsymbol{g}_\text{Rx}^T\ \right] & 0 \cdots 0 \\ & \ddots \ddots \ddots & \\ 0 \cdots & 0 & \left[\ \boldsymbol{g}_\text{Rx}^T\ \right] \end{bmatrix}, \tag{3}$$

with $a_\text{Rx} = (T/M_\text{Rx})^{1/2}$ and $\boldsymbol{g}_\text{Rx} = \big[g_\text{Rx}(-T(N+M_\text{Rx}^{-1})),$ $g_\text{Rx}(-T(N+M_\text{Rx}^{-1}) + T\,M_\text{Rx}^{-1}), \ldots, g_\text{Rx}(T(N+M_\text{Rx}^{-1}))\big]^T$. Furthermore, the M-fold upsampling matrix $\boldsymbol{U}$ with dimensions $N_\text{tot} \times N_\text{q}$ is defined by

$$[\boldsymbol{U}]_{m,n} = \begin{cases} 1, & \text{for} \quad m = M \cdot (n-1) + 1 \\ 0, & \text{else,} \end{cases} \tag{4}$$

where M denotes the effective oversampling factor with respect to the signaling rate, i. e., $M = M_\text{Rx}/M_\text{Tx}$. Afterwards, 1-bit quantization is employed, which yields

$$\boldsymbol{z} = Q_1\,(\boldsymbol{y}) = Q_1\,(\boldsymbol{H}_\text{eff}\, \boldsymbol{p}_x + \boldsymbol{G}_\text{Rx,eff}\, \boldsymbol{n}), \tag{5}$$

where $Q_1(\cdot)$ denotes independent 1-bit quantization of the real and imaginary parts, which is performed element-wise.

A. MMSE Precoding

The optimal MMSE precoding vector $\boldsymbol{p}_\text{x}$ is obtained according to the mean squared error (MSE) criterion under a constrained on the maximum total transmit energy E_0. Considering a scaling factor in the MMSE problem formulation as presented in [13] and taking into account the combined desired output pattern $\boldsymbol{c}_\text{out}$, the design of the space-time MMSE precoder can be cast as the following optimization problem

$$\min_{f,\boldsymbol{p}_\text{x}} \quad \mathbb{E}\left\{\|f(\boldsymbol{H}_\text{eff}\boldsymbol{p}_\text{x} + \boldsymbol{G}_\text{Rx,eff}\boldsymbol{n}) - \boldsymbol{c}_\text{out}\|_2^2\right\} \tag{6a}$$

$$\text{s.t.} \quad \boldsymbol{p}_\text{x}^H \boldsymbol{A}^H \boldsymbol{A} \boldsymbol{p}_\text{x} \leq E_0, \tag{6b}$$

with $\boldsymbol{A} = \left(\boldsymbol{I}_{N_\text{t}} \otimes \boldsymbol{G}_\text{Tx}^T \boldsymbol{U}\right)$ and where $\boldsymbol{G}_\text{Tx}$ denotes a Toeplitz matrix of size $N_\text{tot} \times 3N_\text{tot}$, which is given by

$$\boldsymbol{G}_\text{Tx} = a_\text{Tx} \begin{bmatrix} \left[\ \boldsymbol{g}_\text{Tx}^T\ \right] & 0 \cdots & 0 \\ 0 & \left[\ \boldsymbol{g}_\text{Tx}^T\ \right] & 0 \cdots 0 \\ & \ddots \ddots \ddots & \\ 0 \cdots & 0 & \left[\ \boldsymbol{g}_\text{Tx}^T\ \right] \end{bmatrix}, \tag{7}$$

with $a_\text{Tx} = (T/M_\text{Tx})^{1/2}$ and $\boldsymbol{g}_\text{Tx} = \big[g_\text{Tx}(-T(N+M_\text{Tx}^{-1})),$ $g_\text{Tx}(-T(N+M_\text{Tx}^{-1}) + T\,M_\text{Tx}^{-1}), \ldots, g_\text{Tx}(T(N+M_\text{Tx}^{-1}))\big]^T$.

Following the same derivation as in [13], the optimal solution of (6) is given by

$$\boldsymbol{p}_\text{x,opt} = \frac{1}{f}\left(\boldsymbol{H}_\text{eff}^H \boldsymbol{H}_\text{eff} + \frac{\text{tr}\{\boldsymbol{G}_\text{Rx}^H \boldsymbol{C}_n \boldsymbol{G}_\text{Rx}\}}{E_0} \boldsymbol{A}^H \boldsymbol{A}\right)^{-1} \boldsymbol{H}_\text{eff}^H \boldsymbol{c}_\text{out}, \tag{8}$$

where $\boldsymbol{C}_n$ denotes the noise covariance matrix and the scaling factor is given by $f = \sqrt{\boldsymbol{c}_\text{out}^H \bar{\boldsymbol{\Gamma}}^H \bar{\boldsymbol{\Gamma}} \boldsymbol{c}_\text{out}/E_0}$, with

$$\bar{\boldsymbol{\Gamma}} = \boldsymbol{A}\left(\boldsymbol{H}_\text{eff}^H \boldsymbol{H}_\text{eff} + \frac{\text{tr}\{\boldsymbol{G}_\text{Rx,eff} \boldsymbol{C}_n \boldsymbol{G}_\text{Rx,eff}^H\}}{E_0} \boldsymbol{A}^H \boldsymbol{A}\right)^{-1} \boldsymbol{H}_\text{eff}^H. \tag{9}$$

The reader is referred to [13] for more details on the precoding.

B. Detection

As the design goal of the considered system model is to reduce the complexity at the receiver, the complexity of detection should be low. Hence, we focus on minimum Hamming distance decoding, similar to the works [11]–[13]. In the following, we briefly discuss detection for both considered ZX mappings.

1) Time-Instance Zero-Crossing Detection: For ease of notation, we describe detection for the case $M_\text{Rx} = 3$. Detection for $M_\text{Rx} = 2$ is performed similarly. Following the approach from [12], [13], we introduce the inverse ZX mapping $\overleftarrow{d} : [p_{i-1}, \boldsymbol{c}_{\text{s},i}^T] \to \{0,1\}^2$ (cf. Sec. II-A). Then, to detect the data corresponding to the ith Nyquist interval, we construct a vector $\bar{\boldsymbol{z}}_i = [p_{i-1}, \boldsymbol{z}_i]^T \in \{+1,-1\}^{M_\text{Rx}+1}$, where p_{i-1} corresponds to the last sample of the received sequence from Nyquist interval $(i-1)$ and the vector $\boldsymbol{z}_i$ denotes the M_Rx samples obtained in the ith Nyquist interval.

In the noise-free case, it is possible to detect the segment directly by employing the inverse mapping $\overleftarrow{d}(\cdot)$. However, invalid segments may appear due to noise. Therefore, we make use of minimum Hamming distance decoding, which yields the following detection rule

$$\hat{\boldsymbol{x}}_i = \overleftarrow{d}(\boldsymbol{c}), \quad \text{with} \quad \boldsymbol{c} = \arg\min_{\boldsymbol{c}_\text{map} \in \mathcal{M}} \text{Hamming}(\bar{\boldsymbol{z}}_i, \boldsymbol{c}_\text{map}), \tag{10}$$

where $\boldsymbol{c}_\text{map} = [p_{i-1}, \boldsymbol{c}_{\text{s},i}]^T$, $\mathcal{M}$ denotes all possible forward mappings as specified in [13, Table II], and $\text{Hamming}(\bar{\boldsymbol{z}}_i, \boldsymbol{c}_\text{map})$ denotes the Hamming distance between $\bar{\boldsymbol{z}}_i$ and $\boldsymbol{c}_\text{map}$.

The detection of the first Nyquist interval in the sequence is done taking into account the pilot symbol p_b. Furthermore, note that the real and the imaginary parts can be detected independently in separate processes.

Algorithm 1: Viterbi RLL Sequence Detection

Inputs: K, s_0
Initialization: $\Gamma(s=s_0)=0, \quad \Gamma(s\neq s_0)=\infty$
for $k=0$ *to* $K-1$ **do**
  for $s_{k+1}\in\mathcal{S}_{\mathrm{RLL}}$ **do**
    Update path metric:
    $\Gamma(s_{k+1})=\min_{s_k\in\mathcal{S}_{\mathrm{RLL}}} \Gamma(s_k)+\lambda_k(s_k,s_{k+1})$
    Store survivor sequence:
    $\hat{\boldsymbol{x}}(s_{k+1})=[\hat{\boldsymbol{x}}^T(s_k),\, \breve{\sigma}^T(s_k,s_{k+1})]^T$
  end
end
return $\hat{\boldsymbol{x}}(s_K)$ where $s_K=\arg\min_{s_K\in\mathcal{S}_{\mathrm{RLL}}} \Gamma(s_K)$

2) Runlength-Limited Sequence Detection: For RLL sequence detection, we present a low-complexity minimum Hamming distance Viterbi algorithm [17]. The algorithm is implemented on the time-invariant trellis, which is defined by the FSM RLL encoders given in [7, Table I-II]. Trellis states and transitions are denoted by $s_k\in\mathcal{S}_{\mathrm{RLL}}$ and $(s_k=m, s_{k+1}=m')\in\mathcal{T}_{\mathrm{RLL}}$, respectively. The forward mapping $\sigma(m,m')\in\{+1,-1\}^q$ denotes the output for a transition $(m,m')\in\mathcal{T}_{\mathrm{RLL}}$. Furthermore, $\breve{\sigma}(m,m')\in\{0,1\}^p$ denotes the inverse mapping for a transition $(m,m')\in\mathcal{T}_{\mathrm{RLL}}$, i. e., it specifies the input bits corresponding to this transition. Then, we define the Hamming distance branch metric as

$$\lambda_k(m,m')=\sum_{n=1}^{q}\frac{1}{2}\left|[\boldsymbol{z}]_{(\mathrm{k}-1)\mathrm{q}+(\mathrm{n}-1)}-[\sigma(m,m')]_n\right|, \quad (11)$$

where $[\boldsymbol{z}]_n$ and $[\sigma(m,m')]_n$ denote the nth element of $\boldsymbol{z}$ and $\sigma(m,m')$, respectively. Finally, the minimum Hamming distance Viterbi algorithm is given by Algorithm 1 (cf. [18]), where $K=\frac{NM_{\mathrm{Rx}}}{q}$ and $s_0\in\mathcal{S}_{\mathrm{RLL}}$ denote the number of decoder iterations and the start state, respectively.

IV. Spectral Efficiency

In this section, we obtain a lower bound on the SE for the considered system model. First, we evaluate the average mutual information $\lim_{I_{\mathrm{b}}\to\infty}\frac{1}{I_{\mathrm{b}}}I(\boldsymbol{x}_k;\hat{\boldsymbol{x}}_k)$, where $\boldsymbol{x}_k\in\{0,1\}^{I_{\mathrm{b}}}$ and $\hat{\boldsymbol{x}}_k\in\{0,1\}^{I_{\mathrm{b}}}$ denote the transmitted bit sequence and its estimate at the kth user, both of length I_{b}. In the following, we drop the index k for ease of notation. If the sequence $\boldsymbol{x}$ is i. i. d., then it holds $H(\boldsymbol{x})=\sum_{n=1}^{I_{\mathrm{b}}}H(x_n)$ [19, Th. 2.6.6], where $H(\cdot)$ denotes entropy. Hence, we obtain

$$\begin{aligned}\frac{1}{I_{\mathrm{b}}}I(\boldsymbol{x};\hat{\boldsymbol{x}}) &\overset{(a)}{\geq} \frac{1}{I_{\mathrm{b}}}\sum_{n=1}^{I_{\mathrm{b}}}H(x_n)-\frac{1}{I_{\mathrm{b}}}\sum_{n=1}^{I_{\mathrm{b}}}H(x_n|\hat{x}_n)\\ &=1-\frac{1}{I_{\mathrm{b}}}\sum_{n=1}^{I_{\mathrm{b}}}H_{\mathrm{b}}(\Pr(x_n\neq\hat{x}_n))\\ &\overset{(b)}{\geq} 1-H_{\mathrm{b}}\left(\frac{1}{I_{\mathrm{b}}}\sum_{n=1}^{I_{\mathrm{b}}}\Pr(x_n\neq\hat{x}_n)\right)\triangleq\bar{I}_{\mathrm{LB}}, \quad (12)\end{aligned}$$

where the inequality (a) is due to the chain rule for information [19, Th. 2.5.2], due to independent x_n, and due to the fact that conditioning cannot increase entropy [19, Th. 2.6.5]. The last step, i. e., (b), is due to Jensen's inequality [19, Th. 2.6.2]. Furthermore, $H_{\mathrm{b}}(\cdot)$ denotes binary entropy (cf. [19, eq. (2.1)]) and $\frac{1}{I_{\mathrm{b}}}\sum_{n=1}^{I_{\mathrm{b}}}\Pr(x_n\neq\hat{x}_n)$ corresponds to the uncoded BER.

TABLE I
Considered zero-crossing mapping configurations.

Number of Nyquist intervals per block N = 30				
Precoding	$M_{\mathrm{Tx}}=M_{\mathrm{Rx}}$	I_{b}	O_{s}	Ξ [bit/T/dim]
Time-instance, [13, Table I]	2	45	60	1.5
Time-instance, [13, Table II]	3	60	90	2
RLL $d=1$, [7, Table I]	2	40	60	1.33
RLL $d=2$, [7, Table II]	3	45	90	1.5

Using (12), a lower bound on the SE can be obtained as

$$\mathrm{SE}_{\mathrm{LB}}=\frac{2\cdot\Xi\cdot\bar{I}_{\mathrm{LB}}}{1+\epsilon_{\mathrm{Tx}}}, \quad (13)$$

where the factor 2 in the numerator is due to complex signaling and Ξ denotes the transmission rate of the considered mapping in bit per Nyquist interval per real signaling dimension (cf. Table I). Furthermore, ϵ_{Tx} denotes the roll-off of the raised cosine (RC) transmit filter. Note that in contrast to [5], [6], [8], the SE lower bound in (13) is evaluated w. r. t. a strictly band-limited channel.

V. Numerical Results

Here, we compare the performance of the considered ZX mappings numerically. Simulation parameters are listed in Table I, where I_{b} and O_{s} denote the number of input bits and output symbols per block of N Nyquist intervals. For the RLL mapping, we always choose $d=M_{\mathrm{Tx}}-1$. The SNR is defined as

$$\mathrm{SNR}=\frac{E_0/(NT)}{N_0(1+\epsilon_{\mathrm{Tx}})/T}=\frac{E_0}{NN_0(1+\epsilon_{\mathrm{Tx}})}, \quad (14)$$

where N_0 denotes the noise power spectral density. Simulation results are obtained for a system with $N_{\mathrm{t}}=8$ transmit antennas and $N_{\mathrm{u}}=2$ single-antenna users. The entries of $\boldsymbol{H}$ are i. i. d. zero-mean complex Gaussian distributed with unit variance. The receive and the transmit filters are chosen as a root-raised cosine and RC, respectively; each with roll-off factor $\epsilon_{\mathrm{Rx}}=\epsilon_{\mathrm{Tx}}=0.22$, i. e., parameters are chosen similar to [11]. Furthermore, for all numerical evaluations it holds $M_{\mathrm{Rx}}=M_{\mathrm{Tx}}$.

First, we evaluate the uncoded BER for all ZX mapping configurations from Table I in Fig. 2.a. Comparing the time-instance ZX mapping with $M_{\mathrm{Tx}}=2$ and the RLL ZX mapping with $M_{\mathrm{Tx}}=3$, which both achieve the same transmission rate (cf. Table I), we notice that for SNRs above approx. 10 dB, the RLL ZX mapping achieves a substantially lower uncoded BER. Note that the remaining configurations are difficult to compare, as they result in different transmission rates (cf. Table I).

In Fig. 2.b we evaluate the SE lower bound given in (13). For SNRs below 0 dB, all schemes show a similar performance. The RLL ZX mappings achieve the highest SE for all considered SNRs. However, the encoding and decoding complexity of the RLL ZX mappings is also higher. For SNRs below and above 10 dB, the highest SE is achieved using the RLL mapping with $M_{\mathrm{Tx}}=2$ and $M_{\mathrm{Tx}}=3$, respectively. Surprisingly, the time-instance ZX mapping achieves a higher SE for $M_{\mathrm{Tx}}=2$ as for $M_{\mathrm{Tx}}=3$. This could be caused by increased ISI in case of higher M_{Tx}.

Finally, for $M_{\mathrm{Tx}}=2$, we compare the SE lower bound for the ZX mappings to QP [11]. QP involves zero-forcing spatial pre-coding and per user maximal minimum distance to the decision threshold (MMDDT) codebook optimization [11], i. e., temporal

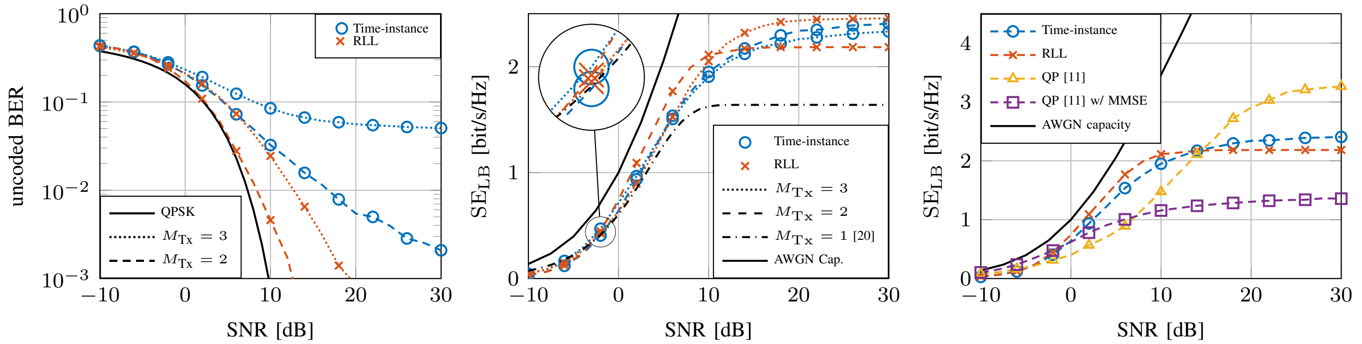

(a) (b) (c)

Fig. 2. For all evaluations it holds $M_{\mathrm{Rx}} = M_{\mathrm{Tx}}$. In (a) we compare the uncoded BER. In (b) we evaluate the lower bound on the SE for a bandlimited channel. All ZX mappings achieve a substantially higher SE as compared to standard QPSK signaling with 1-bit quantization [20]. In (c) we compare the SE lower bound of the considered ZX mappings to QP [11]. We also compare to a modified QP [11] with spatio-temporal MMSE precoding, denoted as *QP w/ MMSE*.

precoding; its performance is depicted in Fig. 2.c. Because MMDDT precoding is known to outperform MMSE precoding at high SNR, whereas MMSE precoding is better at low SNR [13], we also consider a modified version of QP here: We optimize a single codebook for all users w. r. t. the MSE criterion and then employ MMSE precoding from Sec. III-A. This scheme is denoted as *QP w/ MMSE* in Fig. 2.c. The ZX mappings achieve a significantly higher SE as QP with MMSE precoding for $\mathrm{SNR} > 0\,\mathrm{dB}$. This demonstrates the effectiveness of signaling in the time-domain, i. e., encoding the information in the ZXs, as compared to signaling in the amplitude-domain, e. g., using QP, for systems employing 1-bit quantization and oversampling. QP achieves the highest SE at high SNR, which is also partly due to MMDDT precoding. However, in practice, the complexity of QP is prohibitive as it involves optimization and transmission of a codebook for each user and channel realization [11].

VI. Conclusions

In this work, we compared time-instance and runlength-limited (RLL) zero-crossing (ZX) mappings for a multi-user MIMO downlink scenario, where the receivers employ 1-bit quantization and oversampling. The RLL ZX mapping was found to achieve a lower uncoded BER and a higher spectral efficiency (SE), whereas the time-instance ZX mapping offers a lower complexity and an only slightly lower SE. Both considered ZX mappings achieved a significantly higher SE at low SNR compared to quantization precoding [11], while simultaneously offering a lower complexity. This demonstrates the advantage of signaling in the time-domain for systems employing 1-bit quantization and oversampling.

References

[1] A. Al-Fuqaha, M. Guizani, M. Mohammadi, M. Aledhari, and M. Ayyash, "Internet of things: A survey on enabling technologies, protocols, and applications," *IEEE Commun. Surveys Tuts.*, vol. 17, no. 4, pp. 2347–2376, Jun. 2015.

[2] R. H. Walden, "Analog-to-digital converter survey and analysis," *IEEE J. Sel. Areas Commun.*, vol. 17, no. 4, pp. 539–550, Apr. 1999.

[3] S. Shamai, "Information rates by oversampling the sign of a bandlimited process," *IEEE Trans. Inf. Theory*, vol. 40, no. 4, pp. 1230–1236, Jul. 1994.

[4] R. Deng, J. Zhou, and W. Zhang, "Bandlimited communication with one-bit quantization and oversampling: Transceiver design and performance evaluation," *IEEE Trans. Commun.*, vol. 69, no. 2, pp. 845–862, Feb. 2021.

[5] L. T. N. Landau, M. Dörpinghaus, and G. P. Fettweis, "1-bit quantization and oversampling at the receiver: Sequence-based communication," *EURASIP J. Wireless Commun. Netw.*, vol. 2018, no. 1, p. 83, Apr. 2018.

[6] L. Landau, M. Dörpinghaus, and G. Fettweis, "Communications employing 1-bit quantization and oversampling at the receiver: Faster-than-Nyquist signaling and sequence design," in *Proc. IEEE Int. Conf. on Ubiquitous Wireless Broadband (ICUWB)*, Montreal, Canada, Oct. 2015, pp. 1–5.

[7] P. Neuhaus *et al.*, "Sub-THz wideband system employing 1-bit quantization and temporal oversampling," in *Proc. IEEE Int. Conf. Commun. (ICC)*, Dublin, Ireland, Jun. 2020, pp. 1–7.

[8] P. Neuhaus, M. Dörpinghaus, H. Halbauer, V. Braun, and G. Fettweis, "On the spectral efficiency of oversampled 1-bit quantized systems for wideband LOS channels," in *Proc. IEEE Int. Symp. on Personal, Indoor and Mobile Radio Commun. (PIMRC)*, London, UK, Aug. 2020, pp. 1–6.

[9] A. B. Üçüncü and A. Ö. Yılmaz, "Oversampling in one-bit quantized massive MIMO systems and performance analysis," *IEEE Trans. Wireless Commun.*, vol. 17, no. 12, pp. 7952–7964, Dec. 2018.

[10] P. Neuhaus, M. Dörpinghaus, and G. Fettweis, "Oversampled 1-bit quantized wideband systems: Is it better to spend samples in time or in space?" in *Proc. IEEE Int. Workshop on Signal Process. Advances in Wireless Commun. (SPAWC)*, Cannes, France, Jul. 2019, pp. 1–5.

[11] A. Gokceoglu, E. Björnson, E. G. Larsson, and M. Valkama, "Spatio-temporal waveform design for multiuser massive MIMO downlink with 1-bit receivers," *IEEE J. Sel. Topics Signal Process.*, vol. 11, no. 2, pp. 347–362, Mar. 2017.

[12] D. M. V. Melo, L. T. N. Landau, and R. C. de Lamare, "Zero-crossing precoding with maximum distance to the decision threshold for channels with 1-bit quantization and oversampling," in *Proc. IEEE Int. Conf. Acoustics, Speech and Signal Process. (ICASSP)*, Barcelona, Spain, May 2020, pp. 5120–5124.

[13] ——, "Zero-crossing precoding with MMSE criterion for channels with 1-bit quantization and oversampling," in *Proc. Int. ITG Workshop on Smart Antennas (WSA)*, Hamburg, Germany, Feb. 2020, pp. 1–6.

[14] G. Fettweis, M. Dörpinghaus, S. Bender, L. Landau, P. Neuhaus, and M. Schlüter, "Zero crossing modulation for communication with temporally oversampled 1-bit quantization," in *Proc. Asilomar Conf. Signals, Systems, and Computers*, Pacific Grove, CA, USA, Nov. 2019, pp. 207–214.

[15] K. A. S. Immink, *Codes for Mass Data Storage Systems*. Eindhoven, Netherlands: Shannon Foundation Publishers, 2004.

[16] J. E. Mazo, "Faster-than-Nyquist signaling," *Bell Syst. Tech. J.*, vol. 54, no. 8, pp. 1451–1462, Oct. 1975.

[17] A. Viterbi, "Error bounds for convolutional codes and an asymptotically optimum decoding algorithm," *IEEE Trans. Inf. Theory*, vol. 13, no. 2, pp. 260–269, Apr. 1967.

[18] G. D. Forney, "The Viterbi algorithm," *Proc. IEEE*, vol. 61, no. 3, pp. 268–278, Mar. 1973.

[19] T. M. Cover and J. A. Thomas, *Elements of Information Theory*. New York, NY, USA: John Wiley & Sons, 2006.

[20] J. Singh, O. Dabeer, and U. Madhow, "On the limits of communication with low-precision analog-to-digital conversion at the receiver," *IEEE Trans. Commun.*, vol. 57, no. 12, pp. 3629–3639, Dec. 2009.